Chapter 7

Extensions to Three Dimensions

The 2D drift-wave model introduced in Chapter 5 gave insight into the basic physics of energy transfer to subgrid-scale modes due to the shearing action of the $\mathbf{E}\times\mathbf{B}$ velocity. That model does not even attempt to capture the linear physics of ITG-driven instabilities, however, and is therefore of no use for predicting experimental results. A generalization to three dimensions of the parameterized hyperviscosity described in Section 6.2 is proposed here. The hyperviscosity model was inserted into the toroidal gyrofluid code developed by Beer, Dorland and Hammett (Beer et al. 1992; Hammett et al. 1994; Beer 1995), a comprehensive fluid moment code in flux-tube coordinates (Beer et al. 1995), which accurately models the linear physics of ITG-driven instabilities for a wide range of parameters.

The generalized 3D hyperviscosity proposed here correctly accounts for the modification of the effective eddy turnover time due to the fact that eddies in ITG turbulence tend to be highly elongated along the field line. Due to the computational cost of 3D turbulence simulations, a comprehensive study of the performance of this hyperviscosity has yet to be performed. Several simulations are presented here using Numerical Tokamak Project (NTP) test-case parameters that demonstrate that use of this hyperviscosity is capable in this one case of reducing the required resolution for a given accuracy by a factor of 2.

Finally, simulations of a particular high-gradient regime are presented with a saturated spectrum that peaks at an unusually long wavelength ($k_\perp \rho_i \sim 0.03$). This simulation could not be performed on the system currently being used for gyrofluid simulations (a Cray YMP) without the hyperviscosity model. Dorland discovered a shift in the linear ITG physics to longer-wavelength instabilities for high-gradient regimes (private communication), and suggests that this shift may be useful in explaining the experimental results concerning longer-wavelength modes in the near-edge region of the tokamak (Durst et al. 1993).

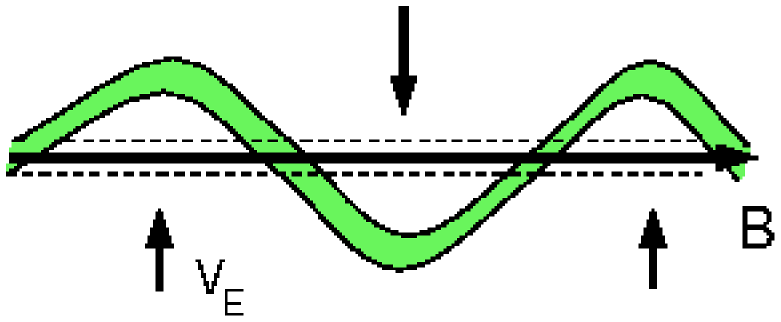

Figure 7.1: The shearing of an eddy in 3D ITG turbulence is illustrated. The dotted lines represent an initial perturbation lined up in the direction of the magnetic field. A small parallel gradient in the $\mathbf{E}\times\mathbf{B}$ velocity quickly results in an eddy with a large parallel wave number.

7.1 3D Hyperviscosity

In 3D ITG turbulence, eddies tend to be highly elongated along the magnetic field lines, so the perpendicular wave number $k_\perp$ is much larger than the parallel wave number $k_{||}$. As the picture in Fig. 7.1 demonstrates, a small deflection due to differences in the $\mathbf{E}\times\mathbf{B}$ velocity at different points along the field line can quickly lead to large parallel wave number. (In the discussion to follow, the variables x and y will be used to represent coordinates perpendicular to the magnetic field and z will be used to represent the coordinate along the field line.) Since the $\mathbf{E}\times\mathbf{B}$ velocity only has perpendicular components, the velocity shear tensor takes the form

$$\boldsymbol{\nabla}\mathbf{V}_{\mathbf{E}\times\mathbf{B}} = \left(\begin{array}{cc|c} \multicolumn{2}{c|}{\multirow{2}{*}{$\boldsymbol{\nabla}_\perp \mathbf{V}_{\mathbf{E}\times\mathbf{B}}$}} & \nabla_{||}\mathbf{V}_{\mathbf{E}\times\mathbf{B}_x} \\ & & \nabla_{||}\mathbf{V}_{\mathbf{E}\times\mathbf{B}_y} \\ \hline 0 & 0 & 0 \end{array}\right). \tag{7.1}$$

Note that some of the components of this tensor are zero, and the parallel gradients are much smaller than the perpendicular ones. One can see from the picture in Fig. 7.1, however, that the elongation of the modes enhances the effect of the parallel shear in the advecting velocity.

A strain rate defined analogously to the one in Eq. (6.7) would effectively ignore any contribution from the parallel gradient terms in taking the mean square of the components of the shear tensor displayed in Eq. (7.1). Splitting the problem into perpendicular and parallel components yields a simple approach for estimating the appropriate damping term for this situation. The perpendicular strain rate $S_\perp$ is given by applying the strain-rate definition (6.7) to the perpendicular component

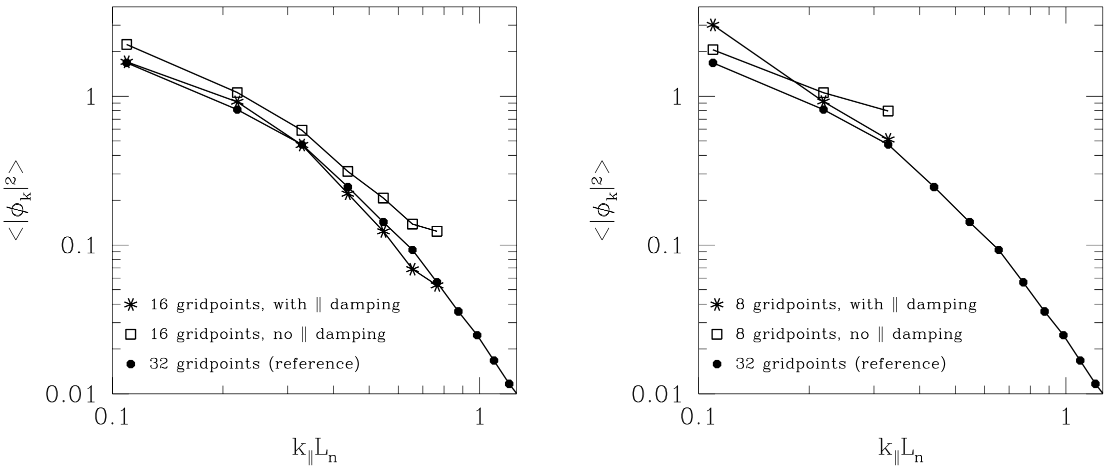

Figure 7.2: Convergence in the number of parallel grid points for the NTP test case with and without the parallel hyperviscosity term.

of the strain tensor $\mathbf{\nabla}_\perp \mathbf{V}_\perp$. The average perpendicular wave number is defined by $k_{\perp \mathrm{av}} = S_\perp / V_{\mathrm{RMS}}$ as in two dimensions [Eq. (6.18)]. A parallel strain rate is defined analogously by

$$S_{||}(x,y,z,t) = \sqrt{\left(\nabla_{||} V_x\right)^2 + \left(\nabla_{||} V_y\right)^2}, \tag{7.2}$$

and so therefore is the average parallel wavenumber $k_{||\mathrm{av}} = S_{||}/V_{\mathrm{RMS}}$. The shearing velocity in k space of a typical eddy due to the parallel gradients scales roughly as $|\mathbf{k}_\perp| \langle S_{||} \rangle$, so the heuristic arguments of Section 6.1.4 suggest that the damping near the cutoff in parallel wave-number space should be of the order $|\mathbf{k}_\perp| \langle S_{||} \rangle / k_{||\mathrm{av}}$. Hence, the form of the subgrid dissipation term for 3D used here is

$$k^2 \nu_{\mathrm{eddy}}(k) = C_{||} \frac{\langle S_{||} \rangle |\mathbf{k}_\perp|}{k_{||\mathrm{av}}} \left(\frac{k_{||}}{k_{||c}} \right)^{p_z} + C_\perp \frac{\langle S_\perp \rangle k_{\perp c}}{k_{\perp \mathrm{av}}} \left[\left(\frac{k_x}{k_{xc}} \right)^{p_x} + \left(\frac{k_y}{k_{yc}} \right)^{p_y} \right]. \tag{7.3}$$

As in the 2D case, the powers should scale with the cutoff wave numbers, $p_x \sim k_{xc}/k_{\perp \mathrm{av}}$, $p_y \sim k_{yc}/k_{\perp \mathrm{av}}$, and $p_z \sim k_{||c}/k_{||\mathrm{av}}$. (For simplicity, the initial study in 3D takes the constant $C_{||} = C_\perp = 0.1$ based on the 2D results and fixes all the powers $p_x = p_y = p_z = 6$ for convenient implementation. Allowing the power to vary may improve the results, but the simulations were performed at fairly low resolutions where the power predicted from the 2D study should be close to 6 anyway, so fixing the powers is a reasonable approximation.)

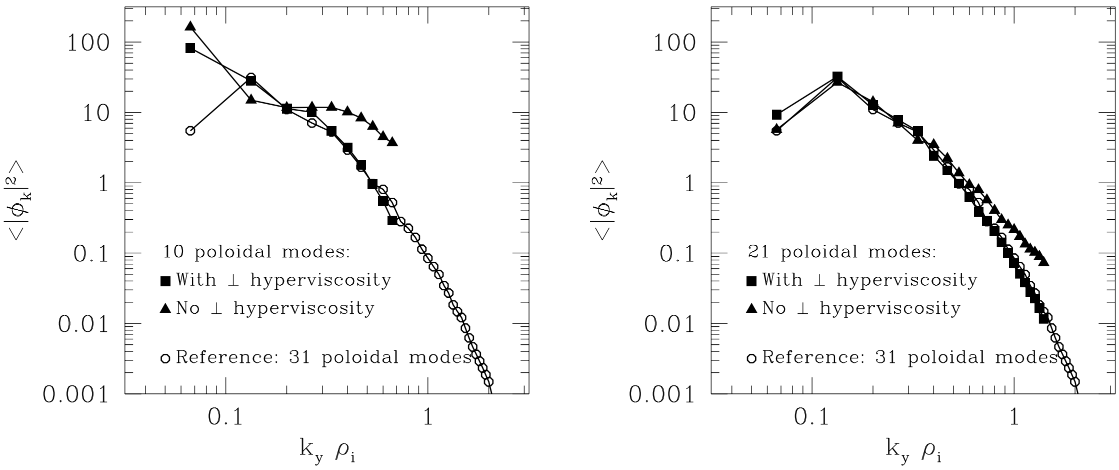

Figure 7.3: Convergence in the number of poloidal modes for the NTP test case with and without the perpendicular hyperviscosity term.

7.2 Numerical Tokamak Project Test Case

The hyperviscosity model was first benchmarked in the toroidal gyrofluid code Griffin on the Numerical Tokamak Project (NTP) Test Case set of parameters taken from TFTR L-mode shot #41309, $\hat{s} = 1.5$, $q = 2.4$, $L_n/R = 0.4$, $\eta_i = 4$, and $T_i = T_e$. Convergence with respect to the physical box size was considered by Beer (1995). Convergence with the number of modes for a fixed box size is examined here.

To test the parallel damping term $C_{||}$, the code was run with 21 poloidal mode numbers, for 8, 16, and 32 points along the field line, with ($C_{||} = 0.1$) and without ($C_{||} = 0$) the parallel damping term. The parallel wave-number spectra for these simulations are shown in Fig. 7.2. Neither of the low-resolution runs with 8 points along the field line have spectra that match the highest-resolution simulation. When the parallel damping term $C_{||}$ is included, the parallel spectrum with 16 grid points is virtually identical to that obtained with 32 points, whereas there are errors at this resolution with no parallel damping. These results indicate that it is possible to save a factor of 2 in resolution in this case while maintaining the same accuracy (provided the largest simulation represents the converged solution).

The code was also run with 10, 21, and 31 poloidal mode numbers, with 16 points along the field line, with and without the perpendicular damping term $C_\perp$. The perpendicular spectra for these simulations are shown in Fig. 7.3. The longest wavelengths in the lowest-resolution simulations show large deviations from the high-resolution simulation, both with and without the damping term. In the medium-resolution simulations, the spectra match the high-resolution spectrum very well both

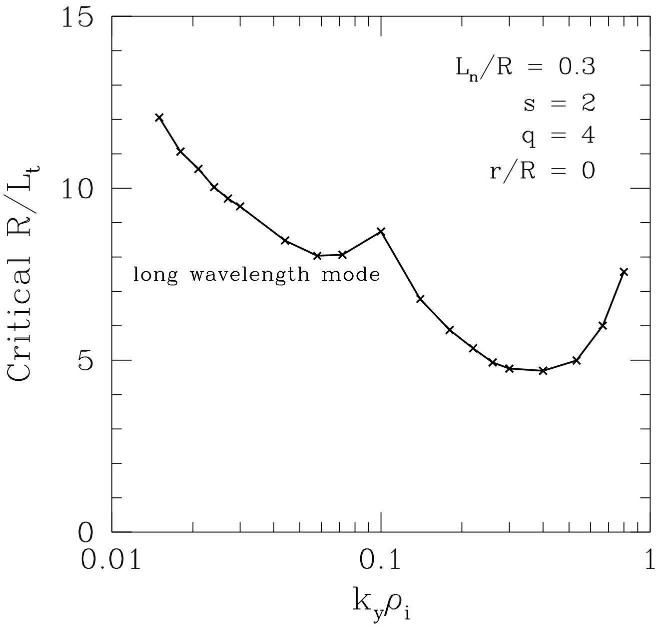

Figure 7.4: Critical temperature gradient of the ITG mode as a function of wave number for a regime with large density gradient. There is a sudden transition at temperature gradients around $R/L_T \sim 8$, at which point significantly longer wavelengths are driven unstable.

with and without the damping term. The perpendicular damping term appears to improve the behavior at short wavelengths, but if one is only interested in accurately modeling the long-wavelength modes responsible for transport, then the new perpendicular hyperviscosity term does not seem to provide any benefit in this case.

7.3 Long-Wavelength Instability

Near the edge of a tokamak, trapped ion effects and large temperature gradients may be a source of drive for long-wavelength instabilities. Calculating the nonlinear evolution of such modes becomes difficult if simulations are required to resolve the peak of the linear growth rate (typically around $|\mathbf{k}_\perp|\rho_i \sim 1/2$). To obtain convergence of simulations without added dissipation, it is often necessary to resolve modes with wavenumbers out to $|\mathbf{k}_\perp|\rho_i \sim 1$ due to unstable modes in this range. This situation is precisely where the hyperviscosity model has the greatest potential for use. It is necessary to eliminate small-scale modes to perform the simulations, but in this case there may not be a sufficient number of resolved damped modes to allow the simulation to saturate.

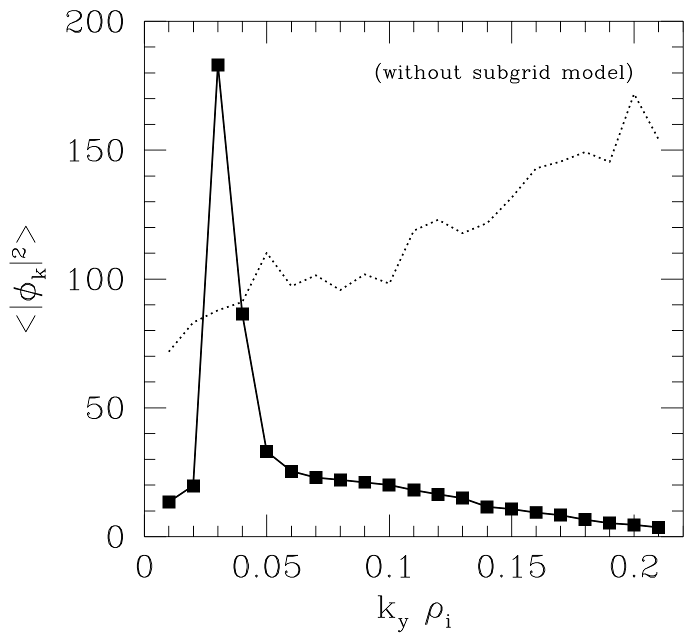

Figure 7.5: Plot of the saturated poloidal spectrum for the simulation discussed in this section. The dotted line indicates the spectrum obtained in a simulation with no subgrid model.

In Fig. 7.4, the critical temperature gradient of the ITG mode is plotted as a function of the poloidal wave number for the parameters $\hat{s} = 2$, $q = 4$, $L_n/R = 0.4$, and $r/R = 0.3$. As the temperature gradient is increased, there is a sudden transition around $R/L_T \sim 8$, at which point significantly longer wavelengths are driven unstable. For most typical parameters (such as the NTP test case in the previous section), the saturated poloidal wave-number spectrum peaks for $k_y\rho_i > 0.1$. In the near-edge region of a tokamak, gradients as large as those considered here are typical, and there is experimental evidence that fluctuations at significantly longer wavelengths $k_y\rho_i \sim 0.05$ are present (Durst et al. 1993).

The edge-like parameters $\hat{s} = 2$, $q = 4$, $L_n/R = 0.1$, $r/R = 0$, $\eta_i = 2$, and $T_i/T_e = 1$ were chosen to test hyperviscosity in this regard. The simulation box had 54 grid points along the field line by 64 points toroidally by 48 points in the radial direction and the $4+2$ moment gyrofluid equations were used. Although the fastest growing linear modes are not resolved, the turbulence saturates and is dominated by long-wavelength modes. The saturated spectrum is shown in Fig. 7.5. Without using any subgrid model in this case, the spectrum tends towards a non-physical equipartition results (the dotted line in the figure). This result can be contrasted

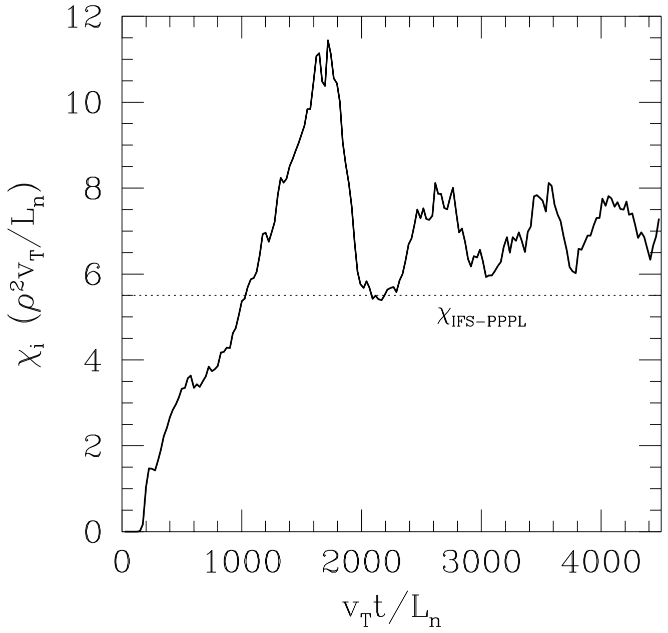

Figure 7.6: Calculated thermal diffusivity for the long-wavelength ITG simulation considered in this section. The dotted line indicates the heat flux predicted by the IFS–PPPL model (Kotschenreuther et al. 1995) for these parameters.

to the NTP test case discussed in the previous section, where a comparable number of modes is capable of resolving enough unstable modes that a subgrid model is unnecessary.

The thermal diffusivity calculated from this simulation is plotted in Fig. 7.6. The dotted line gives a reference diffusivity predicted by the IFS–PPPL model, a mixing-length-based parameterization of the thermal diffusivity that has had significant success in explaining the transport near the core of tokamak discharges. [The value of $\chi_{\mathrm{IFS--PPPL}}$ displayed here is calculated from the formula of Dorland et al. (1994), which differs slightly in the treatment of trapped electron physics from the final "IFS–PPPL" model as reported by Kotschenreuther et al. (1995).] While this simulation has saturated at significantly longer wavelengths than is typical, the predicted heat flux is not significantly higher. (Experimentally measured heat fluxes in the near-edge region are typically much larger than the parameterization. This simulation indicates that the shift to longer-wavelength turbulence may not be responsible for the increased heat flux. More work is necessary to answer this question conclusively, however.)

The actual damping rate produced by the perpendicular part of the hyperviscosity

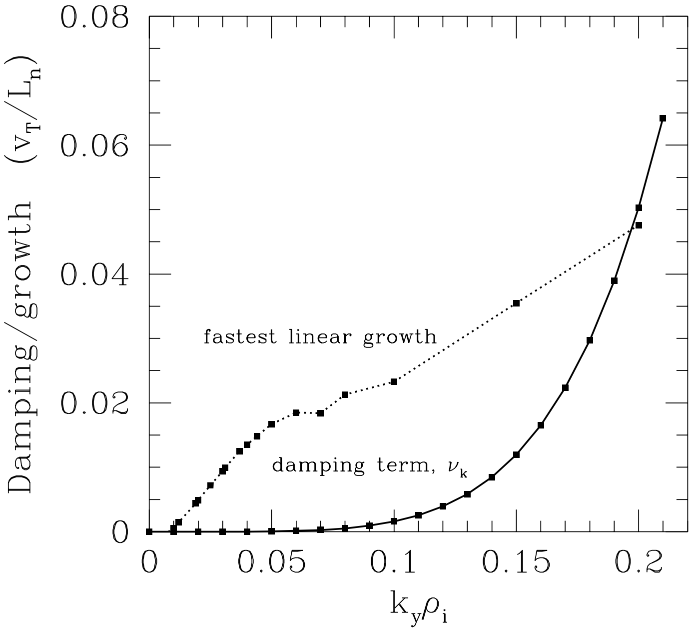

Figure 7.7: Plot of the damping from the hyperviscosity for a given poloidal wave number (with $k_x = 0$) compared with the fastest linear growth rate.

is plotted in Fig. 7.7 against the linear growth rate of the most unstable mode at a given poloidal wave number. The subgrid damping rate is insignificant in comparison to the linear growth rate for most of the resolved modes, including those that form the peak of the saturated spectrum. The damping rate becomes significant only for modes near the cutoff. This comparison serves as a useful check on the consistency of the model. One could question the use of a damping term that has a significant effect on the dominant modes in the saturated spectrum.

7.4 Summary

Heuristic arguments concerning the effect of velocity shear on elongated eddies were used to extend the 2D parameterized hyperviscosity of Eqs. (6.19) and (6.21) to applications in three dimensions where eddies are highly elongated along the additional dimension. This new 3D hyperviscosity [Eq. (7.3)] is essentially the 2D hyperviscosity with the addition of a parallel damping term that scales with parallel velocity shear enhanced by a factor of $|\mathbf{k}_\perp|/k_{||}$.

The 3D hyperviscosity was tested in a comprehensive toroidal gyrofluid turbulence code (Beer 1995). Simulations of the Numerical Tokamak Project Test Case set of parameters indicates that the new heuristically derived parallel damping term can reduce the required parallel resolution by a factor of 2 in some cases. A set of high gradient edge-like parameters were simulated to demonstrate that there are conditions under which the saturated spectrum shifts to significantly longer wavelengths ($k_\theta \rho_i \sim 0.03$). These nonlinear simulations could not be performed without the use of the subgrid damping term proposed here.

To rigorously test the hyperviscosity, one must of course go to higher-resolution simulations. Where higher-resolution simulations are possible, the results considered so far indicate that use of hyperviscosity improves the accuracy of the predicted saturation levels. This model is computationally useful in three ways: it can provide plausible results in situations where a fully resolved simulation is impossible due to time or memory constraints; it can improve the accuracy of resolved simulations; and it can enable one to perform larger numbers of low-resolution simulations for the purpose of parameterizing the heat flux as a function of parameters.